Eur. Phys. J. D **32**, 113–118 (2005)
DOI: 10.1140/epjd/e2004-00183-2

THE EUROPEAN PHYSICAL JOURNAL D

Mapping of the metal intake in plants by large-field X-ray microradiography and preliminary feasibility studies in microtomography

J. Kaiser[1,a], L. Reale[2], A. Ritucci[2], G. Tomassetti[2], A. Poma[3], L. Spanò[3], A. Tucci[3], F. Flora[4], A. Lai[4], A. Faenov[5,b], T. Pikuz[5,b], L. Mancini[6], G. Tromba[6], and F. Zanini[6]

[1] Institute of Physical Engineering, Brno University of Technology, Technická 2896/2, 616 69 Brno, Czech Republic
[2] Physics and Chemistry Departments, University of L'Aquila, gc LNGS INFN, INFM, 67010 Coppito (L'Aquila), Italy
[3] Basic and Applied Biology Department, University of L'Aquila, 67010 Coppito (L'Aquila), Italy
[4] ENEA, Dipartimento Innovazione, Divisione Fisica Aplicata, CRE Frascati, C.P. 65, 00044 Frascati, Italy
[5] MISDC of VNIIFTRI, Mendeleevo, Moscow Region 141 570, Russia
[6] Sincrotrone Trieste SpcA, Strada Statale 14 - km 163,5 in AREA Science Park 34012 Basovizza, Trieste, Italy

Received 2nd August 2004 / Received in final form 21 October 2004
Published online 14 December 2004 –

Abstract. This paper reports on dual energy micro-radiography and tomography techniques applied both to thin plant leaves treated with copper or lead solutions and on Cu-treated small roots and stem sections, performed at the SYRMEP X-ray beamline of ELETTRA synchrotron facility in Trieste (Italy). The features of the source allowed us to apply different imaging techniques with an extremely vast field of view, up to 160×6 mm^2 and 28×6 mm^2 for micro-radiography and tomography experiments, respectively. The feasibility of getting positive indications on metal accumulation in leaves, sections of roots and stems, stem and root whole cylindrical pieces has been checked.

PACS. 87.59.Bh X-ray radiography – 87.59.Fm Computed tomography (CT) – 81.70.Fy Nondestructive testing: optical methods

1 Introduction

The accumulation of metals such as Cu, Zn, As, Cd, Pb, Hg, and others in the environment due to anthropogenic activities is a cause of high health risk because of the possibility that these elements could be transferred to living organisms through fresh water or vegetables. The alarm comes from the high toxicity of these elements, which over given concentrations can affect the plant growth and the animal pastures in contaminated areas, and consequently human exposition down through the food chain.

Among the different solutions, which have been proposed for detecting and removing contaminants, one could be the very expensive chemical removal — the use of chemical compounds that chelate the contaminants [1]. However, the most promising and natural method seems to be the phytoremediation [2]. This technique consists in the removal of contaminants by means of their absorption and accumulation in the roots and leaves of plants, specially cultivated for this purpose and then harvested. Some vegetal species appear to be specialized in the accumulation of particular contaminant atomic species. Moreover, transgenic plants have been obtained recently, with higher accumulation properties [3,4].

The study of these problems presents various aspects, and consists in the detection of contaminants, in the comparison of accumulation properties of various plants and in the mapping of possible biological structures, which can specifically accumulate metals within a given tissue.

Microscopic observation of biological samples is done by means of different X-ray imaging techniques such as X-ray microscopy in the so-called water window, microradiography by absorption and phase contrast imaging [5,6], X-ray fluorescence microprobes [7–10] and fluorescence microtomography [11]. All these techniques have been undertaken with great expectations regarding their potentialities. In order to obtain X-ray images of living samples it is important to optimize the choice of source, optical set-up and type of detector. X-ray microscopy and microradiography investigations make use both of soft X-rays generated by plasma laser sources [12] or synchrotron radiation at rather high photon energies (1−100 keV). In particular, a monochromatic synchrotron radiation beam allows to select a very thin spectral range and, by a specific

[a] e-mail: kaiser@ufi.fme.vutbr.cz
[b] Partly supported by Racah Institute of Physics, Hebrew University, Givat-Ram, Jerusalem 91904, Israel.

optical set-up, to localize in the observed sample the absorption of a given chemical element. This possibility has greatly enhanced the interest of microscopic elemental analysis. X-rays from a synchrotron are in a much higher energy range than the energy of chemical bonds (typically of the order of few eV), so the absorbing electrons are the K or L, M... electrons. Since this absorption is independent from any chemical bond, an absorption measurement can directly give the number of contaminant atoms/cm^2 which are present in the sample.

X-ray dual-energy micro-radiography (i.e. the analysis of the difference between the images obtained above and below the X-ray absorption edges) has been proposed in digital subtraction angiography with monochromatic X-ray sources [13]. In this paper we present such a technique for the detection of accumulation of metal contaminants in plant species resistant to these contaminants, to select candidates to be used for the phytoremediation of soils. As for the identification of the sites of the metals in the leaf, we need to get the largest possible observation field with the highest resolution which can be achieved. In the present experiments we took advantage of the highly-monochromatic, large-field synchrotron radiation in order to detect the heavy-metal accumulation in 2D and 3D biological samples like leaves or plant roots of sizes of several cm^2 and cm^3 respectively.

2 Experimental methods

The main features of third generation synchrotron radiation sources are high intensity and spatial coherence of photons emitted in a small solid angle. This allows to work with short exposure times tuning the photon energy to the sample characteristics and giving the possibility to apply digital subtraction techniques for X-ray imaging. Moreover, as mentioned in the introduction, phase-sensitive techniques can be applied having the additional advantage of allowing imaging of samples with low absorption in respect to hard X-rays, such as light-element composites and biological systems [14,15].

The light source used (SYRMEP beamline) is one of the ELETTRA bending magnets. The horizontal acceptance of the source, covered by the front-end light-port is 7 mrad. The beamline provides, at a distance of about 24 m from the source, a monochromatic, laminar-section X-ray beam with a maximum area of about 160×6 mm^2.

The monochromator, that covers the entire angular acceptance of the beamline, is based on double Si(111) crystals working in Bragg configuration. The useful energy range is 8.3−35 keV. The intrinsic energy resolution of the monochromator is about 2×10^{-3}, caused by the natural divergence of the beam. Typical flux measured at the sample position at 17 keV, at 2 GeV, with a stored beam of 300 mA, is about 1.6×10^8 ph/mm^2 s.

The detector used was a water cooled CCD camera (Photonic Science X-ray Hystar, 2048×2024 full frame, 16 bit, pixel size = 14 μm, field of view 28×28 mm^2) coupled to a Gadolinium Oxysulphide scintillator placed on a straight fibre optic coupler.

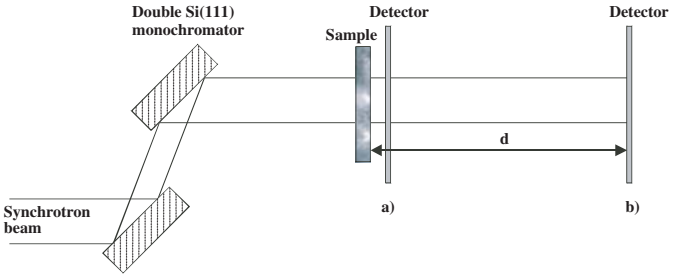

Fig. 1. Experimental set-up used for (a) absorption contrast ($d \approx 0$ m) and (b) phase-sensitive ($d \approx 0.1-2$ m) radiography (PSR) measurements at the SYRMEP beamline.

In the case of radiography (Fig. 1), the sample is illuminated by a monochromatic hard X-ray beam, and a position-sensitive detector is set at a distance d, typically between 1 cm and a few m, from the specimen. If the detector is mounted very close to the sample ($d \approx 0$) we are in the regime of absorption radiography. For higher d values, free space propagation transforms the phase modulation of the transmitted beam into an amplitude modulation. Contrast basically stems from interference between parts of the wavefront that have experienced different phase shifts. According to the choice of the sample-to-detector distance d with respect to the size a of the feature to be identified perpendicularly to the beam direction, one may distinguish between two different regimes: the edge detection regime ($d \ll a^2/\lambda$, where λ is the X-ray wavelength) and the holography regime ($d \approx a^2/\lambda$). The edge detection regime can be used directly to extract morphological information because each border of the phase objects is imaged independently. In the holography regime the objects appear deformed but we can access to the local measure of the phase.

It has been demonstrated that the fine interference structure of phase-images allows detecting very small density and morphological variations in the sample giving contrast in regions of a highly localized change in the refractive index of the specimen, such as its borders or interfaces between the matrix and inclusions. The tomogram is then an outlined image of those domains, while the absorption imaging shows a strongly limited absorption contrast leading to lower signal/noise ratio [13].

An interesting extension of radiography is the X-ray computed micro-tomography (μ-CT) technique (Fig. 2). From an experimental point of view μ-CT is based on the recording of X-ray transmission images (radiographs) on a CCD detector placed at an adjustable distance d from the sample.

Depending on the d value we can distinguish between absorption or phase contrast μ-CT. For each tomography set, according to the sample size, 720 or 1440 projections of the sample are acquired for equally spaced rotation angles and measurement time of the order of 1 s, over a total rotation of 180 degrees. These parameters were previously optimized for absorption and resolution by imaging several samples under different conditions. During a tomography measurement, the 2D radiographs are stored in a PC.

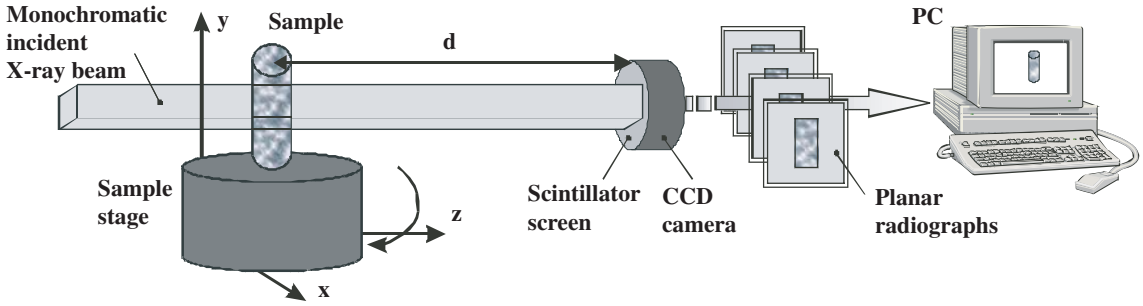

Fig. 2. Experimental set-up for absorption and PS μ-CT at the SYRMEP beamline.

Such tomography projections have been elaborated using a set of routines written in the IDL language [14]. These routines allow the reconstruction of single slices; data can then be saved in several formats and subsequently loaded by other applications for visualization and analysis. The slice reconstruction is performed using a *filtered backprojection algorithm* [13] and in the end a 3D image of the sample is obtained [14]. Therefore, this technique is capable of producing, in a non-invasive way, a 3D digital map of an object. The numerical value of each voxel in the map is related to the X-ray absorption coefficient of the material present in the voxel itself. The distribution of zones of different chemical composition inside a sample can be promptly visualized and quantitatively measured.

3 Results and discussion

The biological samples which we investigated are of various types: (a) leaves or sections of leaves and (b) roots or sections of roots. The thickness of the leaf samples varied from 50 microns to 1 mm, but sections could also be obtained with the desired thickness, to optimize the image contrast. The transversal dimensions of leaves varied from 1 mm to 3 cm.

We proposed to use monochromatic radiation at the wavelengths λ_{AR} and λ_{AL} close to the absorption edge of a given chemical element in order to obtain the precise localization of that element in the observed sample. This was possible by repeating the measurements both on the left and right side of the absorption edge, and by subtracting each-one of the images obtained in the two cases. In Figure 3 the feature of absorption processes in dependence of photon energy for copper (solid curve) and lead (dashed curve) is shown. A jump of attenuation length between point 1 and 2 corresponds to the K-shell absorption edge of Cu and a jump between point 3 and 4 corresponds to the L-shell absorption edge of Pb.

To obtain the map of deposition of the given chemical element inside the sample from the differential images, totally five image expositions should be acquired for any investigated sample area:

- two images I_R and I_L of the irradiated sample using a monochromatic radiation at the wavelength λ_{AR} above and λ_{AL} below the absorption edge, respectively;

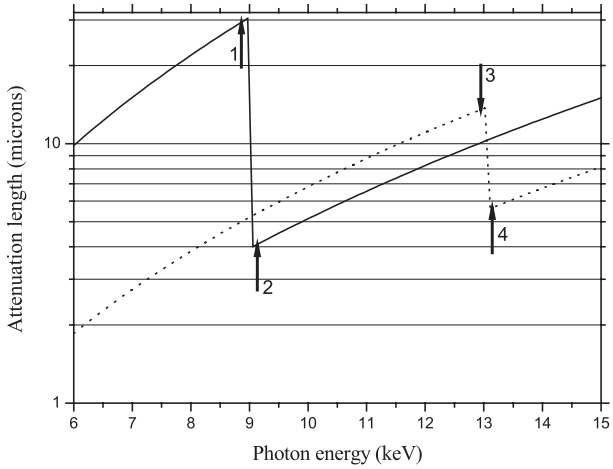

Fig. 3. Attenuation length for the two selected elements Cu (solid line) and Pb (dotted line). The arrows shows the photon energies utilized in differential imaging, 1: 8.90 keV, 2: 9.05 keV and 3: 12.975, 4: 13.150 for the detection of Cu and Pb accumulation, respectively.

- images F_R and F_L, which represents the flat images (images without the samples) taken by the appropriate synchrotron radiation at the wavelength λ_{AR} and λ_{AL}, respectively;
- the background D measured by running the CCD camera without opening the beamline last shutter.

The exposure time t_{exp} strongly depends on the sample; its values were determined by preliminary measurements during the alignment of the set-up: all five measurements were fixed identically. In all our experiments t_{exp} was in the order of a few seconds. The resulting differential image is calculated as:

$$DIF = LOG_R - LOG_L, \tag{1}$$

where LOG_R and LOG_L are the logarithm of the normalized images on the right and left side of the absorption edge defined by:

$$LOG_R = \log\left(\frac{I_R - D}{F_R - D}\right), \tag{2a}$$

$$LOG_L = \log\left(\frac{I_L - D}{F_L - D}\right). \tag{2b}$$

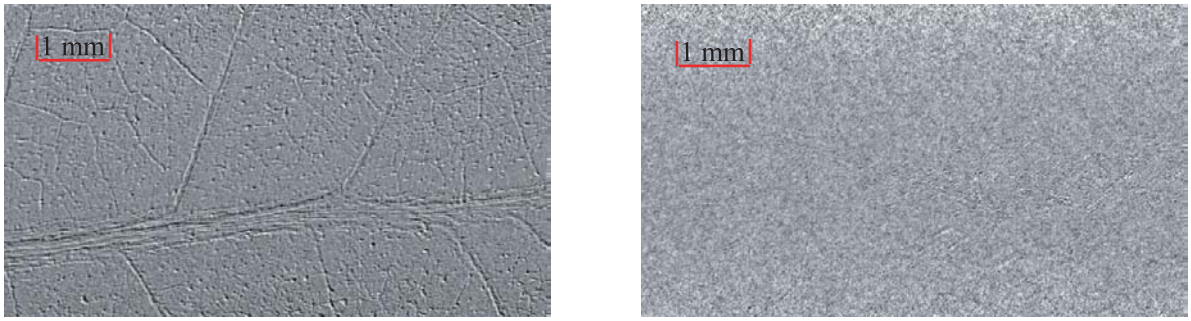

Fig. 4. Pb detection by dual energy (13.150−12.975 keV), phase-contrast imaging at $d = 168$ cm in *Helianthus annuus* leaf, 15 days 10 mM PbAc treated (a), compared with untreated control sample (b).

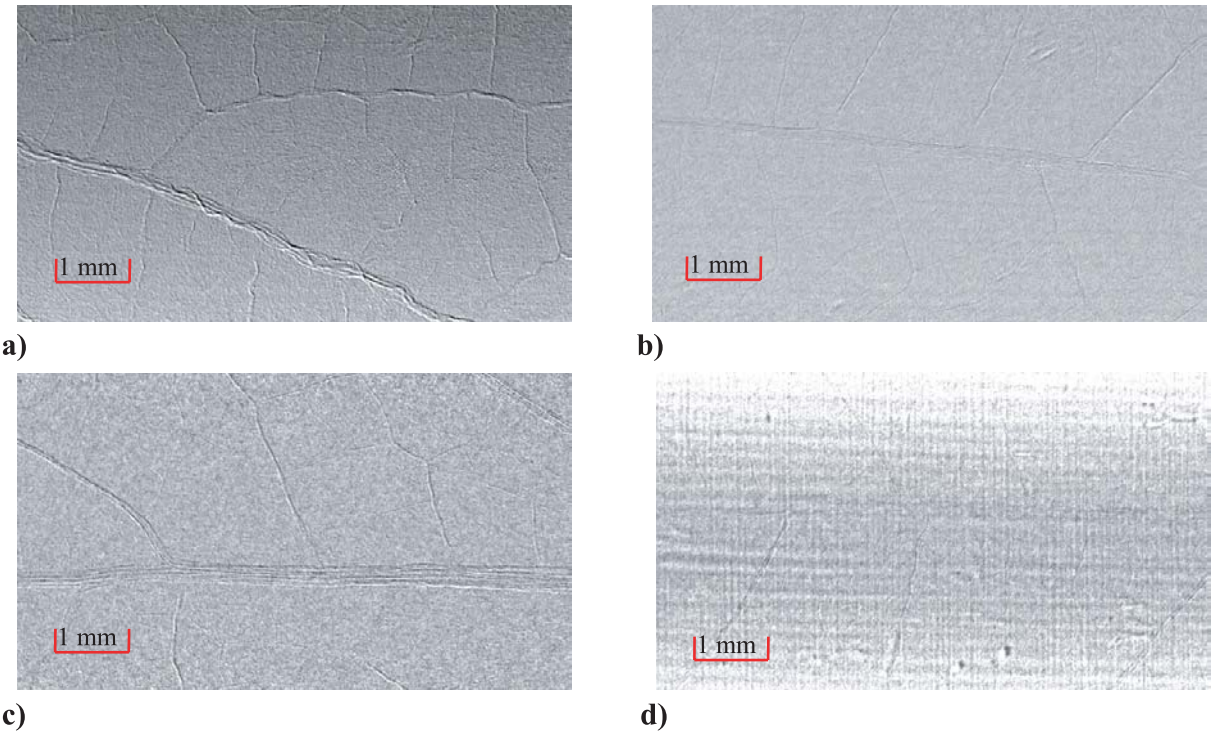

Fig. 5. Cu detection by dual energy (9.05−8.90 keV) phase-contrast imaging at $d = 35$ cm in *Phaseolus vulgaris* leaf, 15 days 10 mM $CuSO_4$ treated ethanol-fixed (a), compared with untreated ethanol-fixed control sample (b) together with 15 days 10 mM $CuSO_4$ treated air dried sample (c), and untreated air-dried control sample (d).

This way, the map of the metal contamination in the investigated sample can be found by an equivalent thickness X_{eq} which produces approximately an absorption contrast greater then ∼20% between the lower-edge and higher-edge images.

In the present measurements the spatial resolution was limited by the pixel size of the CCD detector to 14 μm. Here should be noted that higher spatial resolution (up to ∼1 micron) can be reached using X-ray films.

We investigated the accumulation of Cu (K-edge 8.979 keV) and Pb (L-edge 15.861 keV) both in control (untreated) and treated (grown in solution containing these elements) samples by comparing absorption and phase-contrast radiography (Fig. 1) and tomography (Fig. 2) techniques. We used the dual energy analysis in absorption or phase contrast at the K or L edges of those two elements to prove their uptake in the leaves of treated plants. Typical results for phase-contrast and absorption-contrast techniques are shown in Figures 4−7.

In the investigation of lead accumulation ability of plants, similar leaves of *Helianthus annuus* picked from control samples and from plants treated by PbAc solution (10 mM concentration during 15 days), were irradiated by synchrotron beam at wavelength $\lambda_{AR} = 0.955$ Å (the photon energy of 12.975 keV) and $\lambda_{AL} = 0.942$ Å (the photon energy of 13.150 keV). The detector was placed at a distance of 168 cm from the investigated sample, utilizing phase-contrast technique. Measurements have been done according to the method described above. Figures 4a and 4b show the resulting differential images, calculated

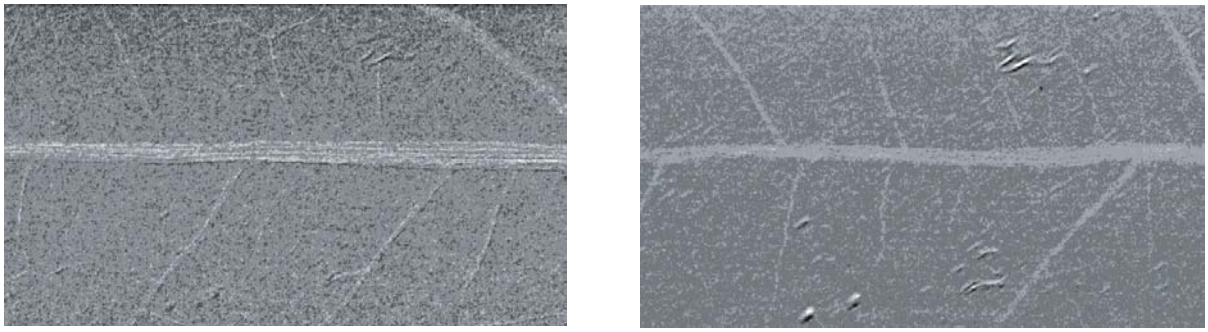

a) b)

Fig. 6. Cu detection by dual energy (9.05−8.90 keV) absorption imaging at $d = 2$ cm in *Phaseolus Vulgaris* leaf, 15 days 10 mM $CuSO_4$ treated ethanol-fixed (a), compared with air-dried sample (b).

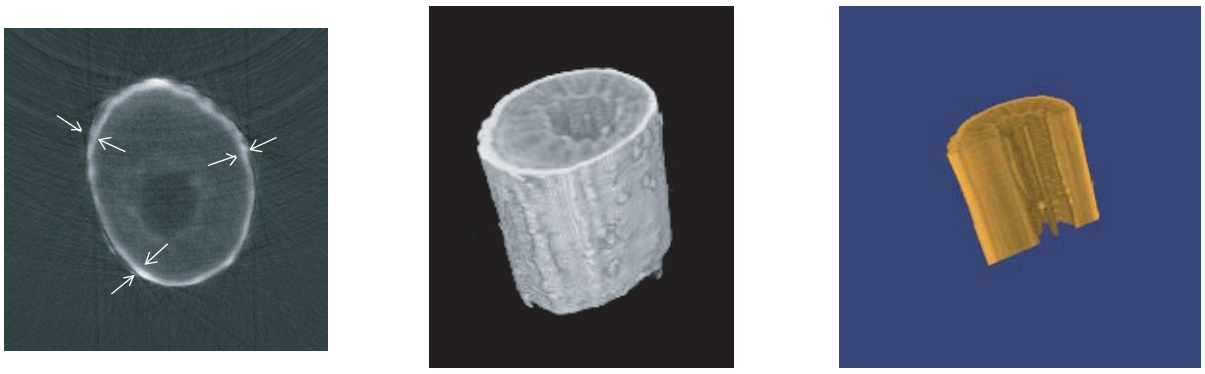

a) b) c)

Fig. 7. Preliminary results on the 3D reconstruction of a root of *Dyplotaxis erucoides* grown in 2% $CuSO_4$ solution; (a) differential planar radiograph, (b) and (c) reconstructions of the root fragments. The white arrows indicate the location of the Cu accumulation.

from equation (1), for treated and control samples correspondingly. Comparing with the resulting differential image of the control leaf (Fig. 4b), the differential image of treated leaf (Fig. 4a) contains a structure indicating the presence of a different absorption at the two wavelengths. Such structure is mostly located on the veins of the leaf and indicates a dominant role of veins for accumulation of Pb.

Similar results have been obtained in the measurements reported in Figure 5. In this case the detector was placed at a distance of 35 cm (phase contrast) for Cu intake detection in *Phaseolus vulgaris* leaves.

Analyzing the differential images obtained with dual-energy phase-contrast analysis (Figs. 4 and 5) we find that both control (i.e. samples without treatment) differential images do not show any pronounced structure. The faint structure, which can be slightly distinguished in Figures 5b and 5d is caused by a phase-effect on the veins of the leaf. On the contrary the differential images obtained for the treated samples show the presence of the clear structure with contaminants.

Utilizing dual-energy absorption contrast analysis, significant differences between the images of Cu treated and untreated control samples were observed. The structure of the veins was clearly visible only on the differential images of treated leaves. As an example, Figure 6 shows the results of the absorption contrast analysis for 15 days 10 mM $CuSO_4$ treated ethanol fixed (Fig. 6a) and air dried (Fig. 6b) Phaseolus vulgaris samples. The detector in these measurements was placed at a distance $d = 2$ cm from the sample.

Utilizing the μ-CT technique *Dyplotaxis erucoides* samples grown in 2% $CuSO_4$ solution were examined. The part of the root with a diameter of ∼3 mm and length ∼10 mm was placed at a distance $d = 20$ cm from the source, therefore the phase-contrast μ-CT configuration was used.

Figure 7 demonstrates the preliminary results of the application of the phase contrast μ-CT techniques for the study of metal intake inside the plants. The white arrows on the differential planar radiograph (Fig. 7a) indicate the ring created by the Cu-accumulation inside the root. On the 3D reconstruction of the root-fragment of *Dyplotaxis erucoides* (Figs. 7b and 7c) the main components of the plant are clearly observable. Figure 7a shows a high concentration of Cu in the external part of roots. In fact, according to Tilston [16] roots are the sites of a preferential Cu accumulation when external Cu supply is large. For Knezek [17] high quantities of Cu produce an impaired

lignification of cell walls. In wheat the effect of lignification is even clearer in the sclerenchyma cells.

4 Conclusions

In conclusion, we report on some X-ray experimental techniques investigating metal-intake inside the plants. Utilizing dual energy micro-radiography or tomography techniques, the distribution-map of the studied metal in the sample was obtained. We took advantage of the features of third generation synchrotron radiation source at SYRMEP beamline of Elettra Synchrotron in Trieste (Italy). The features of the source, mainly the high intensity of photons emitted in a small solid angle and the wide field of view, allowed us to work with short exposure times tuning the photon energy to the sample characteristics without scanning the plane samples. The capability of this method was demonstrated on mapping copper and lead intake in plants grown in controlled conditions. The results show that dual-energy micro-radiography and tomography techniques can be very helpful to find where plants, used for phytoremediation, preferentially accumulate heavy metals. From the biological point of view these techniques are important because they allow us to select the most convenient plants for accumulation of metals in air-biomass to increase the efficiency of phytoremediation in fields. From a physical point of view the sensitivity to metal intake experimented for instance for Cu at the photon energy $\sim$9 keV of these preliminary experiments is $\sim$200 μg/cm^2; but we should note that this is not the optimum energy for so thin biological samples. Because the linear absorption coefficient jump at the absorption edges scales with the third power of the photon energy at the edge, as shown in Henke's tables [18] and the transmission of a biological material for a thickness of 0.1$-$0.5 mm is sufficient even at a photon energy of 1$\div$2 keV, we expect that a sensitivity in the order of few μg/cm^2 can be achieved.

So the possibility of further improvement, relaying mainly on the use of the lower photon energy not available at the moment on this X-ray line; and the use of carefully calibrated samples, foresee the possibility of reaching higher accuracy appropriate even for analytical measurements.

This work was supported by the ELETTRA Synchrotron facility, by the European Community (under EU contract HPRI-CT-1999-00033), by the Italian National Institute of Nuclear Physics and by the Italian National Institute of Matter Physics. J. Kaiser acknowledges the Ministry of Education of Czech Republic (Grant J22/98:26L100002) and the Czech Science Foundation (Grant GACR 202/02/P113). We thank Dr. Gianfelice Cinque and Antonio Grilli of Frascati National laboratory for their excellent advice in the preparation of the experiment, and Erasmus students Tamás Egri of Brno University of Technology and Federica Di Michele of L'Aquila University for their active support in our research.

References

1. Annual Status Report of Treatment Technologies for Site Cleanup-U.S: Environmental Protection Agency (EPA) (2000)
2. M.M. Lasat, J. Environ. Qual. **31**, 109 (2002)
3. U. Kramer, A. Chardonnens, Appl. Microbiol. Biotechnol. **55**, 661 (2001)
4. A.A. Kamnev, D. van der Lelie, Bioscence Rep. **20**, 239 (2000)
5. A. Snigirev, I. Snigireva, V. Kohn, S. Kuznetsov, I. Schelokov, Rev. Sci. Instrum. **66**, 5486 (1995)
6. P. Cloetens, E. Boller, W. Ludwig, J. Baruchel, M. Schlenker, Europhys. News **32**, 46 (2001)
7. S.R. Sutton, S. Bajt, J. Delaney, D. Schulze, S. Tokunaga, Rev. Sci. Instrum. **66**, 1464 (1995)
8. W. Yun, S.T. Pratt, R.M. Miller, Z. Cai, D.B. Hunter, A.G. Jarstfer, K.M. Kemner, B. Lai, H.R. Lee, D.G. Legnini, W. Rodrigues, C.I. Smith, J. Synchrotron Rad. **5**, 1390 (1998)
9. J.E. Penner, Peariso, K. Hahn, Sync. Rad. News **5**, 22 (2000)
10. S. Hayakawa, S. Tohno, K. Takagawa, M. Suzuki, T. Hirokawa, Nucl. Instr. Meth. A **901**, 467 (2001)
11. C.G. Schroer, B. Benner, T.F. Gunzler, M. Kuhlmann, B. Lengeler, W.H. Schroder, A.J. Kuhn, A.S. Siminovici, A. Snigirev, I. Snigireva, *Developments in X-ray Tomography III*, *Proc. SPIE 4503*, 2002, edited by U. Bonse, p. 230
12. C. Tillman, I. Mercer, K. Herrlin, S. Svanberg, J. Opt. Soc. Am. B **13**, 209 (1996)
13. N.F. Gmur, D. Chapman, W. Tomlinson, A.C. Thompson, W.M. Lavender, K. Scalia, N. Malloy, J. Jacob, Rev. Sci. Instrum. **66**, 1357 (1995)
14. F. Montanari, SYRMEP TOMO Project, tutorial (2003)
15. G.T. Herman, *Image reconstruction from projections* (Academic Press, New York, 1980)
16. G.H. Tilstone, M.R. Macnair, Ann. Botany **80**, 747 (1997)
17. B. Knezek, in *Plant Mineral Nutrition and Membrane Transport*, Chapter: *Copper: Physiology and crop nutrition*, `http://www.msu.edu/course/css/853/Copper.html` (1997)
18. B.L. Henke, E.M. Gullikson, J.C. Davis, At. Data Nucl. Data Tables **54**, 181 (1993)